Int. J. Heat Mass Transfer. Vol. 32, No. 1, pp. 121–130, 1989
Printed in Great Britain

0017–9310/89 $3.00 + 0.00

Numerical prediction of flow characteristics and retardation of mixing in a turbulent swirling flow

SHUICHIRO HIRAI, TOSHIMI TAKAGI and TERUYOSHI HIGASHIYA
Department of Mechanical Engineering, Faculty of Engineering, Osaka University, Suita, Osaka 565, Japan

(*Received* 7 *September* 1987 *and in final form* 26 *April* 1988)

Abstract—Numerical predictions are compared with the experiments of turbulent swirling flow and mixing in a stationary pipe. Two kinds of turbulence models, the k–ε two equation model and the stress/flux equation model, are employed in the present calculations. The axial and tangential velocity profiles and the characteristics of the retardation of mixing in the presence of the swirl can be predicted by the stress/flux equation model, whereas the k–ε two equation model fails in this respect. Comprehensible interpretations of the phenomena, especially of the retardation of turbulent transport of momentum and species (He) due to swirl, are presented.

1. INTRODUCTION

TURBULENT swirling flows are often encountered in many furnaces and combustors as well as in fluid machinery. In these flow fields, turbulent transport of heat, mass and momentum are significantly influenced by swirl. Swirl is known to have two contradictory effects, i.e. promotion and suppression of turbulent transport of heat, mass and momentum. This paper aims to obtain a better understanding and to establish the prediction procedures of the characteristics of turbulent swirling flow including mixing. Numerous experimental and numerical studies have been conducted in order to investigate the effects of swirl on heat, mass and momentum transport.

The turbulent swirling flow produced in a pipe rotating around its axis is one of the fundamental swirling flows where the swirls suppress the turbulent transport of heat [1] and momentum [2]. In these flow fields, characteristic phenomena due to the swirl, such as the laminarization phenomena [2] or the heat transfer deterioration [1] have been pointed out. The present authors showed that these phenomena can be predicted by employing the stress/flux equation model [3, 4]. The dominant factors of the laminarization phenomena and the heat transfer deterioration were revealed by the calculations [3, 4].

On the contrary, the authors studied the turbulent swirling flow in which the turbulent transport of heat and momentum are promoted by the swirl [5]. Experimental and numerical studies of heat and momentum transport in a concentric annulus with a rotating inner cylinder have been conducted, and the causes of promoting the heat and the momentum transport were elucidated [5].

Various computations of turbulent swirling flows were conducted using turbulence models with and without modifications related to the effects of the swirls. Launder *et al.* [6] and Leschziner and Rodi [7] calculated boundary layer flows developing over curved and spinning surfaces and strongly swirling free jets, respectively, introducing the swirl-related modifications into the k–ε two equation model. Launder and Morse [8], and Gibson and Younis [9] computed swirling jets employing the stress equation model. However, there has been no report on the computations of turbulent swirling flow including mixing in a confined circular tube.

It is known that the standard k–ε two equation model fails to predict the turbulent swirling flow field in a confined tube [10, 11]. Kobayashi and Yoda proposed a modified k–ε model with the hypothesis of anisotropy and turbulence [11]. As for the experiments of turbulent swirling flow with mixing in a stationary pipe, the phenomena of the retardation of mixing due to the swirl were revealed [12, 13].

In the present study, numerical predictions were compared with the experiments of refs. [13, 14] of turbulent swirling flow and mixing of He with air in a stationary pipe. Two kinds of turbulence models, standard k–ε two equation model and stress/flux equation model, were employed in the present calculations. The applicability of the turbulence models is examined paying attention to the retardation of turbulent transport of momentum and species due to the swirl, and the interpretations of the turbulent transport characteristics in relation with swirl are presented.

2. ANALYSIS

2.1. *Basic equations*

The analysis is based on the time-averaged conservation equations of mass, momentum and species in an axisymmetric cylindrical coordinate system, with and without swirl. There is no recirculating zone due

NOMENCLATURE

C'_T, C'_2, C_D constants in k–ε turbulence model
$C_1, C_2, C_{\varepsilon 1}, C_{\varepsilon 2}, C_\varepsilon, C_{1c}, C'_{1c}, C_{2c}, C_c$ constants in stress/flux equation model
$C_{\overline{uv},i}, C_{\overline{vw},i}, C_{\overline{vm},i}$ convection terms in stress/flux equation model
D diffusion coefficient
$D_{\overline{uv},i}, D_{\overline{vw},i}, D_{\overline{vm},i}$ diffusion terms in stress/flux equation model
k turbulent kinetic energy
M, m time-mean and fluctuating mass fraction of He
p time-mean pressure
$P_{\overline{uv},i}, P_{\overline{vw},i}, P_{\overline{vm},i}$ production terms of stress/flux equation model
$R_{\overline{uv},i}, R_{\overline{vw},i}, R_{\overline{vw},i}$ redistribution terms of stress/flux equation model
R distance from the central axis
U, V, W time-mean velocity components in the x-, r-, θ-directions
u, v, w fluctuating velocity components in the x-, r-, θ-directions
U^+ non-dimensional velocity, U/U^*
U^* friction velocity
x, r coordinates
X axial distance from the nozzle tip
XD axial distance from the inlet cross section of calculations
y^+ non-dimensional wall distance.

Greek symbols
α, β, γ constants in stress/flux equation model
ε dissipation rate of k
μ_l laminar viscosity
μ_t turbulent viscosity
ν_l kinematic viscosity
ρ density
$\sigma_k, \sigma_\varepsilon, \sigma_m$ diffusion constants in k–ε model
τ_w wall shear stress.

Subscripts
l laminar
t turbulent
w wall.

Superscript
$\bar{}$ time averaging.

to the swirl and the boundary layer approximation is applied. The basic equations are

$$\frac{\partial}{\partial x}(r\rho U) + \frac{\partial}{\partial r}(r\rho V) = 0 \tag{1}$$

$$\rho\left(U\frac{\partial U}{\partial x} + V\frac{\partial U}{\partial r}\right) = -\frac{\partial p}{\partial x} - \frac{1}{r}\frac{\partial}{\partial r}(r\rho\overline{uv}) + \frac{1}{r}\frac{\partial}{\partial r}\left(r\mu_l\frac{\partial U}{\partial r}\right) \tag{2}$$

$$\rho\left(U\frac{\partial W}{\partial x} + V\frac{\partial W}{\partial r} + \frac{VW}{r}\right) = -\frac{1}{r^2}\frac{\partial}{\partial r}(r^2\rho\overline{vw}) + \frac{1}{r^2}\frac{\partial}{\partial r}\left\{\mu_l r^3\frac{\partial}{\partial r}\left(\frac{W}{r}\right)\right\} \tag{3}$$

$$\frac{\partial p}{\partial r} = -\frac{\partial}{\partial r}\rho\overline{v^2} + \frac{\rho}{r}(W^2 + \overline{w^2} - \overline{v^2}) \tag{4}$$

$$\rho\left(U\frac{\partial M}{\partial x} + V\frac{\partial M}{\partial r}\right) = -\frac{1}{r}\frac{\partial}{\partial r}(r\rho\overline{vm}) + \frac{1}{r}\frac{\partial}{\partial r}\left(r\rho D\frac{\partial M}{\partial r}\right) \tag{5}$$

where x, r are the coordinates in the axial and radial directions, respectively. U, V, W and u, v, w are the time-mean and fluctuating velocity components in the axial, radial and tangential directions, respectively. M and m are the time-mean and fluctuating mass fraction of species (He), respectively, ρ the fluid density, μ_l the laminar viscosity, D the diffusion coefficient, p the pressure. ρ and μ_l are evaluated from the concentration of species (He). An overbar (¯) denotes the time average. The transport of momentum and species (He) by turbulent motion, represented by correlations between fluctuating quantities in equations (2)–(5) are evaluated from the turbulence models.

2.2. *The turbulence models*

The turbulence models employed in the present calculations in order to estimate the Reynolds stresses or the turbulent flux of species are the standard k–ε two equation model [15] and the stress/flux equation model [16, 17].

In the k–ε two equation model, kinetic energy of turbulence k and its dissipation rate ε are calculated from the following transport equations [15]:

$$\rho\left(U\frac{\partial k}{\partial x} + V\frac{\partial k}{\partial r}\right) = \frac{1}{r}\frac{\partial}{\partial r}\left(r\frac{\mu_{\text{eff}}}{\sigma_k}\frac{\partial k}{\partial r}\right) + \mu_t\left[\left\{r\frac{\partial}{\partial r}\left(\frac{W}{r}\right)\right\}^2 + \left(\frac{\partial U}{\partial r}\right)^2\right] - \rho\varepsilon \tag{6}$$

$$\rho\left(U\frac{\partial \varepsilon}{\partial x} + V\frac{\partial \varepsilon}{\partial r}\right) = \frac{1}{r}\frac{\partial}{\partial r}\left(r\frac{\mu_{\text{eff}}}{\sigma_\varepsilon}\frac{\partial \varepsilon}{\partial r}\right) + \frac{\varepsilon}{k}\left[C'_1\mu_t\left\{\left(r\frac{\partial}{\partial r}\left(\frac{W}{r}\right)\right)^2 + \left(\frac{\partial U}{\partial r}\right)^2\right\} - C'_2\rho\varepsilon\right]. \tag{7}$$

The turbulent viscosity μ_t is determined from the relation $\mu_t = \rho C_D k^2/\varepsilon$. The empirical constants in the k–ε two equation model are adopted from refs. [15, 18, 19] and are listed as follows:

$$C_D = 0.09, \quad C_1' = 1.45, \quad C_2' = 1.95,$$

$$\sigma_k = 1.0, \quad \sigma_\varepsilon = 1.3.$$

The turbulent transport terms $\rho\overline{uv}$, $\rho\overline{vw}$ and $\rho\overline{vm}$ in equations (2), (3) and (5) are related to the gradients of the time-mean flow quantities and they are modelled as $\rho\overline{uv} = -\mu_t \partial U/\partial r$, $\rho\overline{vw} = -\mu_t r\partial(W/r)/\partial r$ and $\rho\overline{vm} = -\mu_t/\sigma_m \partial M/\partial r$. Here, σ_m is the turbulent Schmidt number and takes the value of 0.7 in the present calculation.

The stress/flux equation model adopted in the present study is that proposed by Launder *et al.* [16]. But for the diffusive transport term (the triple velocity correlation term), the present study applies the simpler form approximated by Daly and Harlow [20]. The flux equation model employed in the present study is that proposed by Launder [17]. The stress/flux equation model is composed of transport equations of six correlations of the velocity fluctuations ($\overline{u^2}$, $\overline{v^2}$, $\overline{w^2}$, $\overline{uv}$, $\overline{uw}$, $\overline{vw}$), of the dissipation rate ε and of three correlations of velocity fluctuation and mass concentration fluctuation ($\overline{um}$, $\overline{vm}$, $\overline{wm}$). These transport equations are described as follows in the axisymmetric cylindrical coordinate system, applying the boundary layer approximation:

$$U\frac{\partial \overline{u^2}}{\partial x} + V\frac{\partial \overline{u^2}}{\partial r} = -2\overline{uv}\frac{\partial U}{\partial r} - C_1\frac{\varepsilon}{k}\left(\overline{u^2} - \tfrac{2}{3}k\right) + 2\alpha\overline{uv}\frac{\partial U}{\partial r} + \tfrac{2}{3}(\alpha+\beta)P + \frac{C_s}{r}\frac{\partial}{\partial r}\left(\frac{rk\overline{v^2}}{\varepsilon}\frac{\partial \overline{u^2}}{\partial r}\right) - \tfrac{2}{3}\varepsilon \tag{8}$$

$$U\frac{\partial \overline{v^2}}{\partial x} + V\frac{\partial \overline{v^2}}{\partial r} - 2\overline{vw}\frac{W}{r} = 2\overline{vw}\frac{W}{r} - C_1\frac{\varepsilon}{k}\left(\overline{v^2} - \tfrac{2}{3}k\right) - 2\alpha\overline{vw}\frac{W}{r} + 2\beta\left(\overline{vw}\frac{\partial W}{\partial r} + \overline{uv}\frac{\partial U}{\partial r}\right) + \tfrac{2}{3}(\alpha+\beta)P + \frac{C_s}{r}\frac{\partial}{\partial r}\left\{\frac{rk}{\varepsilon}\left(\overline{v^2}\frac{\partial \overline{v^2}}{\partial r} - 2\frac{\overline{vw^2}}{r}\right)\right\} - 2\frac{C_s}{r}\frac{k}{\varepsilon}\left\{\overline{vw}\frac{\partial \overline{vw}}{\partial r} + \frac{\overline{w^2}(\overline{v^2} - \overline{w^2})}{r}\right\} - \tfrac{2}{3}\varepsilon \tag{9}$$

$$U\frac{\partial \overline{w^2}}{\partial x} + V\frac{\partial \overline{w^2}}{\partial r} + 2\overline{vw}\frac{W}{r} = -2\overline{vw}\frac{\partial W}{\partial r} - C_1\frac{\varepsilon}{k}\left(\overline{w^2} - \tfrac{2}{3}k\right) + 2\alpha\overline{vw}\frac{\partial W}{\partial r} - 2\beta\overline{vw}\frac{W}{r} + \tfrac{2}{3}(\alpha+\beta)P + \frac{C_s}{r}\frac{\partial}{\partial r}\left\{\frac{rk}{\varepsilon}\left(\overline{v^2}\frac{\partial \overline{w^2}}{\partial r} + 2\frac{\overline{vw^2}}{r}\right)\right\} + 2\frac{C_s k}{r\varepsilon}\left\{\overline{vw}\frac{\partial \overline{vw}}{\partial r} + \frac{\overline{w^2}(\overline{v^2} - \overline{w^2})}{r}\right\} - \tfrac{2}{3}\varepsilon \tag{10}$$

$$U\frac{\partial \overline{uv}}{\partial x} + V\frac{\partial \overline{uv}}{\partial r} - \overline{uw}\frac{W}{r} = -\overline{v^2}\frac{\partial U}{\partial r} + \overline{uw}\frac{W}{r} - C_1\frac{\varepsilon}{k}\overline{uv} + \alpha\left(\overline{v^2}\frac{\partial U}{\partial r} - \overline{uw}\frac{W}{r}\right) + \beta\left(\overline{u^2}\frac{\partial U}{\partial r} + \overline{uw}\frac{\partial W}{\partial r}\right) - \gamma k\frac{\partial U}{\partial r} + \frac{C_s}{r}\frac{\partial}{\partial r}\left\{\frac{rk}{\varepsilon}\left(\overline{v^2}\frac{\partial \overline{uv}}{\partial r} - \frac{\overline{vw}\,\overline{uw}}{r}\right)\right\} - \frac{C_s k}{r\varepsilon}\left(\overline{vw}\frac{\partial \overline{uw}}{\partial r} + \overline{w^2}\frac{\overline{uv}}{r}\right) \tag{11}$$

$$U\frac{\partial \overline{uw}}{\partial x} + V\frac{\partial \overline{uw}}{\partial r} + \overline{uv}\frac{W}{r} = -\left(\overline{uv}\frac{\partial W}{\partial r} + \overline{vw}\frac{\partial U}{\partial r}\right) - C_1\frac{\varepsilon}{k}\overline{uw} + \alpha\left(\overline{uv}\frac{\partial W}{\partial r} + \overline{vw}\frac{\partial U}{\partial r}\right) - \beta\overline{uv}\frac{W}{r} + \frac{C_s}{r}\frac{\partial}{\partial r}\left\{\frac{rk}{\varepsilon}\left(\overline{v^2}\frac{\partial \overline{uw}}{\partial r} + \frac{\overline{vw}\,\overline{uv}}{r}\right)\right\} + \frac{C_s}{r}\frac{k}{\varepsilon}\left\{\overline{vw}\frac{\partial \overline{uv}}{\partial r} - \overline{w^2}\frac{\overline{uw}}{r}\right\} \tag{12}$$

$$U\frac{\partial \overline{vw}}{\partial x} + V\frac{\partial \overline{vw}}{\partial r} + (\overline{v^2} - \overline{w^2})\frac{W}{r} = -\left(\overline{v^2}\frac{\partial W}{\partial r} - \overline{w^2}\frac{W}{r}\right) - C_1\frac{\varepsilon}{k}\overline{vw} + \alpha\left(\overline{v^2}\frac{\partial W}{\partial r} - \overline{w^2}\frac{W}{r}\right) - \beta\left(\overline{v^2}\frac{W}{r} - \overline{uw}\frac{\partial U}{\partial r} - \overline{w^2}\frac{\partial W}{\partial r}\right) - \gamma k\left(\frac{\partial W}{\partial r} - \frac{W}{r}\right) + \frac{C_s}{r}\frac{\partial}{\partial r}\left\{\frac{rk}{\varepsilon}\left(\overline{v^2}\frac{\partial \overline{vw}}{\partial r} + \overline{vw}\frac{(\overline{v^2} - \overline{w^2})}{r}\right)\right\} + \frac{C_s k}{r\varepsilon}\left\{\overline{vw}\frac{\partial}{\partial r}(\overline{v^2} - \overline{w^2}) - 4\overline{w^2}\frac{\overline{vw}}{r}\right\} \tag{13}$$

$$U\frac{\partial \varepsilon}{\partial x} + V\frac{\partial \varepsilon}{\partial r} = C_{\varepsilon 1}\frac{\varepsilon P}{k} - C_{\varepsilon 2}\frac{\varepsilon^2}{k} + \frac{C_\varepsilon}{r}\frac{\partial}{\partial r}\left(\frac{rk\overline{v^2}}{\varepsilon}\frac{\partial \varepsilon}{\partial r}\right) \tag{14}$$

$$U\frac{\partial \overline{um}}{\partial x} + V\frac{\partial \overline{um}}{\partial r} = -\left(\overline{uv}\frac{\partial M}{\partial r} + \overline{vm}\frac{\partial U}{\partial r}\right) + C_{2c}\overline{vm}\frac{\partial U}{\partial r} - C_{1c}'\frac{\varepsilon}{k}\left\{\frac{1}{k}(\overline{uv}\cdot\overline{vm} + \overline{uw}\cdot\overline{wm} + \overline{u^2}\cdot\overline{um}) - \tfrac{2}{3}\overline{um}\right\} + \frac{\partial}{\partial r}C_c\frac{k}{\varepsilon}\left(\overline{v^2}\frac{\partial \overline{um}}{\partial r} + \overline{uv}\frac{\partial \overline{vm}}{\partial r} - \frac{1}{r}\overline{uw}\cdot\overline{wm}\right) - C_{1c}\frac{\varepsilon}{k}\overline{um} + C_c\frac{k}{\varepsilon}\frac{1}{r}\left(\overline{uv}\frac{\partial \overline{vm}}{\partial r} + \overline{v^2}\frac{\partial \overline{um}}{\partial r} - \frac{1}{r}\overline{uw}\cdot\overline{wm}\right) \tag{15}$$

$$U\frac{\partial\overline{vm}}{\partial x}+V\frac{\partial\overline{vm}}{\partial r}-\frac{w}{r}\overline{wm}=-\left(\overline{v^2}\frac{\partial M}{\partial r}-\frac{1}{r}\overline{wm}\cdot W\right)$$
$$+\frac{2}{r}C_c\frac{k}{\varepsilon}\left(\overline{v^2}\frac{\partial\overline{vm}}{\partial r}-\overline{vw}\frac{\partial\overline{wm}}{\partial r}\right)+2\frac{\partial}{\partial r}C_c\frac{k}{\varepsilon}\left(\overline{v^2}\frac{\partial\overline{vm}}{\partial r}\right.$$
$$\left.-\frac{1}{r}\overline{vw}\cdot\overline{wm}\right)-\frac{2}{r^2}C_c\frac{k}{\varepsilon}(\overline{w^2}\cdot\overline{vm}+\overline{vw}\cdot\overline{wm})$$
$$-C_{1c}\frac{\varepsilon}{k}\overline{vm}-C'_{1c}\frac{\varepsilon}{k}\left\{\frac{1}{k}(\overline{v^2}\cdot\overline{vm}+\overline{vw}\cdot\overline{wm}+\overline{uv}\cdot\overline{um})\right.$$
$$\left.-\tfrac{2}{3}\overline{vm}\right\}-C_{2c}\frac{\overline{wm}}{r}W \qquad (16)$$

$$U\frac{\partial\overline{wm}}{\partial x}+V\frac{\partial\overline{wm}}{\partial r}+\frac{w}{r}\overline{vm}=-\left(\overline{vw}\frac{\partial M}{\partial r}+\overline{vm}\frac{\partial W}{\partial r}\right)$$
$$-C_{1c}\frac{\varepsilon}{k}\overline{wm}+C_{2c}\overline{vm}\frac{\partial W}{\partial r}-C'_{1c}\frac{\varepsilon}{k}\left\{\frac{1}{k}(\overline{vw}\cdot\overline{vm}\right.$$
$$\left.+\overline{w^2}\cdot\overline{wm}+\overline{uw}\cdot\overline{um})-\tfrac{2}{3}\overline{wm}\right\}+3C_c\frac{k}{\varepsilon}\left\{\frac{1}{r}\overline{vw}\frac{\partial\overline{vm}}{\partial r}\right.$$
$$\left.+\frac{1}{r}\overline{v^2}\frac{\partial\overline{wm}}{\partial r}+\frac{1}{r^2}\overline{vw}\cdot\overline{vm}-\frac{1}{r^2}\overline{w^2}\cdot\overline{wm}\right\}$$
$$+\frac{\partial}{\partial r}C_c\frac{k}{\varepsilon}\left(\overline{v^2}\frac{\partial\overline{wm}}{\partial r}+\overline{vw}\frac{\partial\overline{vm}}{\partial r}+\frac{1}{r}\overline{vw}\cdot\overline{vm}\right.$$
$$\left.-\frac{1}{r}\overline{w^2}\cdot\overline{wm}\right) \qquad (17)$$

where

$$P=-\overline{uv}\partial U/\partial r-\overline{vw}r\partial(W/r)/\partial r.$$

The empirical constants in the stress/flux equation model are adopted from Launder *et al.* [16], Hanjalic and Launder [21], Morse [22] and Launder [17] and are listed as follows:

$$C_1=1.5,\quad C_2=0.4,\quad C_s=0.22,\quad C_{\varepsilon1}=1.45,$$
$$C_{\varepsilon2}=1.90,\quad C_\varepsilon=0.15,\quad C_{1c}=3.8,\quad C'_{1c}=-2.2,$$
$$C_{2c}=0.33,\quad C_c=0.11.$$

2.3. *The boundary conditions and the calculation procedure*

At the near wall boundaries, the boundary conditions are determined for the grid point in a turbulent region one mesh inside the wall. Near the wall region, the non-dimensional velocity $U^+(=U/U^*)$ and the non-dimensional distance from the wall $y^+(=U^*y/\nu_l)$ are assumed to obey a universal relation $U^+=f(y^+)$ in a fully developed turbulent flow. Here, U^* denotes the friction velocity $(=(\tau_w/\rho)^{0.5})$, τ_w the wall shear stress, y the distance from the wall and $\nu_l=\mu_l/\rho$. The von Karman universal velocity distribution [23] is applied for the relation, $U^+=f(y^+)$. In application of this relationship to the swirling flow, the composed velocity of the axial velocity component U and the tangential velocity W is used instead of U in the universal velocity distribution relation noted above and in this case, τ_w becomes a composed wall shear stress. From these relations, the boundary conditions of U and W near the wall region are evaluated and the wall shear stress is also evaluated. The boundary value for the turbulent kinetic energy near the wall region is evaluated from the relation $k=\tau_w/(\rho C_D^{0.5})$ derived from the local equilibrium assumption.

In the calculation employing the k–ε two equation model, the boundary value for the dissipation rate ε near the wall region is obtained from the assumption of the local equilibrium of equation (6) and from the boundary value for k.

In the calculation employing the stress/flux equation model, the velocity fluctuation correlations $\overline{u^2}$, $\overline{v^2}$ and $\overline{w^2}$ are evaluated dividing the turbulent kinetic energy k $(=(\overline{u^2}+\overline{v^2}+\overline{w^2})/2)$ in the ratio 1.05 : 0.42 : 0.53, respectively, which are estimated from the experiment [14]. The boundary value for the dissipation rate ε near the wall region is evaluated from the assumption that it is in equilibrium with the production term in the transport equation of k. The boundary conditions for $\overline{uw}$ are evaluated from equation (12), with the approximation of $\partial/\partial x\ll\partial/\partial r$, $V=0$ and neglecting the diffusive transport. The boundary values for the velocity fluctuation correlations $\overline{uv}$ and $\overline{vw}$ near the wall region are evaluated from the wall shear stress of the axial direction component $(\tau_{xr})_w$ and of the tangential direction component $(\tau_{r\theta})_w$, respectively, which are the components of the composed wall shear stress τ_w.

The boundary conditions of M, $\overline{um}$, $\overline{vm}$ and $\overline{wm}$ near the wall region are that the gradients of M, $\overline{um}$, $\overline{vm}$, $\overline{wm}$ in the radial direction are zero.

The inlet profiles of U, W, k, $\overline{u^2}$, $\overline{v^2}$, $\overline{w^2}$, M are evaluated from the experiments. $\overline{uv}$, $\overline{vw}$ and $\overline{uw}$ are given by linear profiles connecting the boundary value near the wall region with the zero value at the central axis. The dissipation rate, ε is determined from the turbulent kinetic energy k and the length scale. $\overline{um}$, $\overline{vm}$ and $\overline{wm}$ are evaluated solving transport equations (15)–(17), respectively, with other dependent variables fixed in the initial profiles.

The above differential equations are solved numerically using a finite difference method based on the procedure developed by Patanker and Spalding [24]. Thirty grid points are located in the radial directions at non-uniform intervals.

3. RESULTS AND DISCUSSIONS

The effects of the swirl on the characteristics of turbulent flow and mixing in a stationary pipe were studied experimentally [13, 14]. Turbulent swirling air flow was formed in a pipe of 60 mm i.d. and He was coaxially injected from a round tube nozzle of 7 mm i.d. installed at the central axis. The radial profiles

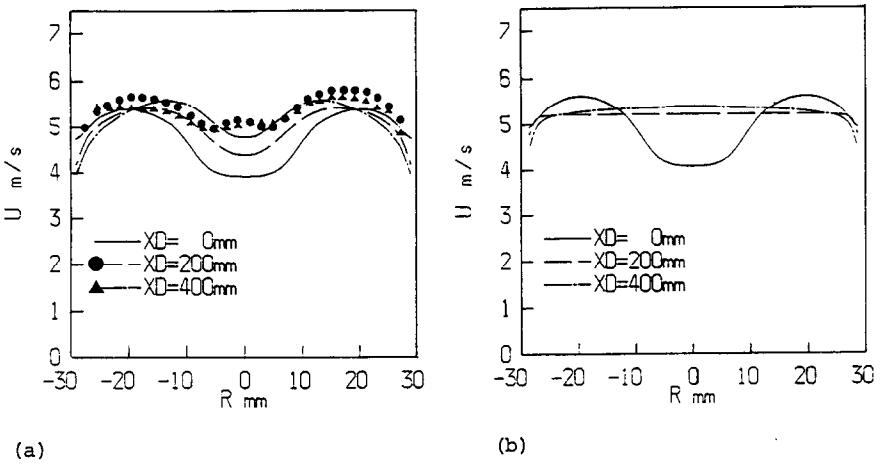

FIG. 1. Comparison of experimental and calculated axial velocity profile. Plots, Yamada's experimental results [14]. Lines, predictions: (a) stress/flux equation model; (b) k–ε two equation model.

of axial velocity U and tangential velocity W were measured by a laser Doppler velocimeter (LDV) at the cross sections of 100, 300, and 500 mm downstream from the nozzle tip [14]. The concentration profiles of He were measured on the axis and in the cross sections of 100, 200 and 500 mm downstream from the nozzle tip. The concentration of He was analyzed by a gas chromatograph after gas sampling by a probe. It was pointed out that:

(1) the axial velocity U retains the radial profile depressed near the central axis at the downstream region in the swirling flow;

(2) the tangential velocity W becomes the solid-body rotational profile near the central axis and the free vortex profile at the outer region;

(3) the retardation of the turbulent mixing occurs due to the swirl as compared with the mixing in the non-swirling flow in the region more than 100 mm downstream from the nozzle tip.

In the present study, numerical computations were conducted employing the k–ε two equation model and the stress/flux equation model. The computations were compared with the above mentioned experiments to examine the applicability of the turbulence models to the swirling flow, putting the check points on the turbulent swirling flow characteristics and the retardation of the mixing due to the swirl. The causes of the characteristic phenomena due to the swirl were also investigated.

In Fig. 1, the experimental and the calculated radial profile of the axial velocity U are compared. Plotted points in Fig. 1(a) are Yamada's experimental results [14]. XD denotes the distance from the inlet cross section of the calculation. The inlet cross section ($XD = 0$) of the calculation is selected 100 mm downstream from the nozzle tip where the measured data are available and the density nonuniformity is not significant. The lines in Figs. 1(a) and (b) are the predictions employing the stress/flux equation model and the k–ε two equation model, respectively. R is the distance from the central axis. The inlet conditions of the calculations are equal to the experimental ones at $XD = 0$. The experimental axial velocity U (plotted points in the figure) retains the radial profile depressed near the central axis at the downstream region (Fig. 1(a), $XD = 200$, 400 mm). However, the calculated axial velocity employing the k–ε two equation model becomes flattened rapidly (Fig. 1(b)). The rapid flattening is caused by the overestimation of the turbulent flux of the axial momentum. The axial momentum is excessively transported toward the central axis in the calculation employing the k–ε model as compared with the experimental results. The calculation employing the stress/flux equation model, however, can predict the tendency of the measured axial velocity which retains the profile depressed near the central axis at the downstream region ($XD = 200$ and 400 mm). The experimental axial velocity U shows a protruded profile near the central axis whereas the calculation employing the stress flux equation model fails to predict this experimental tendency. This disagreement seems to be small as compared with the overall agreement of the experimental and calculated profiles of the axial velocity U (Fig. 1(a)). This overall agreement is caused by the fact that the calculation employing the stress/flux equation model estimates the turbulent transport of axial momentum toward the central axis less than that of the k–ε model. The causes for the retardation of momentum flux $\rho\overline{uw}$ obtained by the stress/flux equation model as compared with that by the k–ε model, can be investigated by evaluating the magnitude of the terms in transport equation (11) of $\overline{uw}$.

The radial profiles of the magnitude of the terms in equation (11) at the cross section of $XD = 200$ mm are indicated in Fig. 2. The marks in the figure $P_{\overline{uw},i}$, $R_{\overline{uw},i}$, $C_{\overline{uw},i}$, $D_{\overline{uw},i}$ ($i = 1, 2, \ldots$), indicate the terms in equation (11), which are shown beside Fig. 2, respectively.

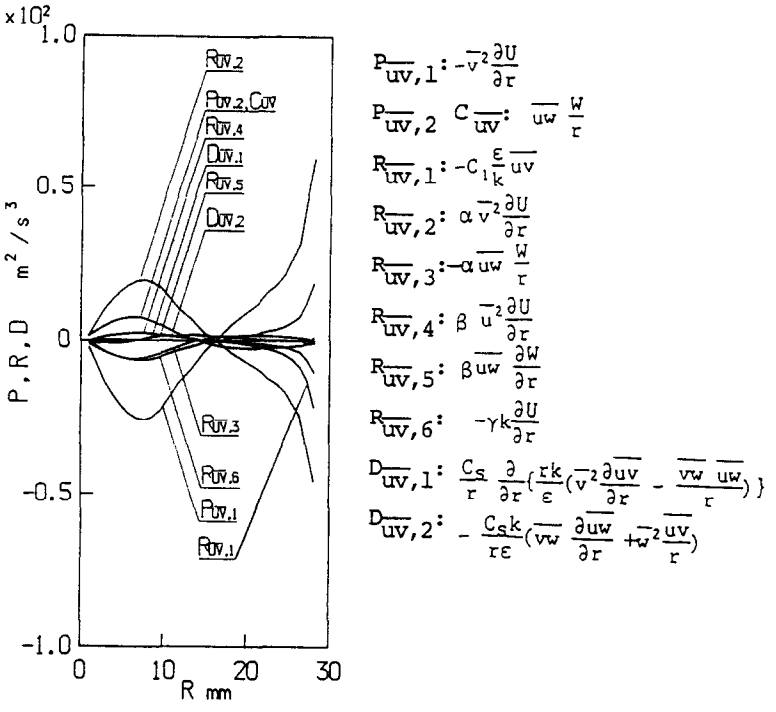

FIG. 2. Calculated radial profile of the magnitude of the terms in the transport equation of $\overline{uv}$.

$P_{\overline{uv},i}$ is the production term. $P_{\overline{uv},1}$ $(= -\overline{v^2}\partial U/\partial r)$ is concerned with the radial gradient of axial velocity U and takes a negative value in the region where the axial velocity shows a depressed profile $(\partial U/\partial r > 0)$. Then $P_{\overline{uv},1}$ has a tendency for the axial momentum to be transported toward the central axis and for the axial velocity U to recover the depressed profile. The redistribution term $R_{\overline{uv},2}$ $(= \alpha\overline{v^2}\partial U/\partial r)$ has the reverse effect against the production term $P_{\overline{uv},1}$ $(= -\overline{v^2}\partial U/\partial r)$. But the coefficient α takes the value 0.76, which means that $R_{\overline{uv},2}$ never overcomes the effect of $P_{\overline{uv},1}$. Particularly, in the case with the swirl, $P_{\overline{uv},2}$ $(= \overline{uw}W/r)$ including the tangential velocity component has a sign opposite to $P_{\overline{uv},1}$, which retards the turbulent transport of axial momentum toward the central axis. $R_{\overline{uv},4}$ $(= \beta\overline{u^2}\partial U/\partial r)$ has the same effect but it is much smaller than that of $P_{\overline{uv},2}$. According to these considerations, the stress equation model contains the production term $P_{\overline{uv},2}$ $(= \overline{uw}W/r)$, which contributes to predict well the axial velocity profiles obtained in the experiments. The same term $C_{\overline{uv}}$ $(= \overline{uw}W/r)$ is contained in the convection terms.

In Fig. 3, the predicted radial profiles of the tangential velocity W are compared with the experimental values. Plotted points in Fig. 3(a) are the experimental results of Yamada [14]. The lines in Figs. 3(a) and (b) are the calculated results employing the stress/flux equation model and the k–ε model, respectively. The inlet conditions of the calculations $(XD = 0)$ are equal to the experimental ones at $XD = 0$. The experimental tangential velocity W retains a solid-body rotational profile near the central axis and a free-vortex profile at the outer region (Fig. 3(a)). The experimental tangential momentum increases slightly in the downstream region which might arise from experimental errors. The measured tangential velocity profiles show clearly the solid-body rotational profile near the central axis and the free vortex profile at the outer region. These characteristic profiles of tangential velocity are obtained in other flow conditions, where CO_2 is injected from the nozzle instead of He [14]. The calculated tangential velocity employing the k–ε model becomes a solid-body rotational profile rapidly in almost all flow regions. That is to say, the tangential momentum is rapidly transported toward the pipe wall in the calculation employing the k–ε model and the solid-body rotational profile without the free vortex region becoming stable.

The calculation employing the stress/flux equation model, however, can predict the experimental tendency, that is, the tangential velocity retains the solid-body rotational profile near the central axis and the free vortex profile at the outer region in the downstream region ($XD = 200$ and 400 mm). The causes of the good prediction are elucidated by investigating the magnitude of the terms in the transport equation of $\overline{vw}$ which prescribes the profile of the tangential velocity W.

The radial profiles of the magnitude of the terms in the transport equation of $\overline{vw}$ (equation (13)) at the cross section of $XD = 200$ mm are indicated in Fig. 4. The marks in the figure $P_{\overline{vw},i}$, $R_{\overline{vw},i}$, $C_{\overline{vw},i}$, $D_{\overline{vw},i}$

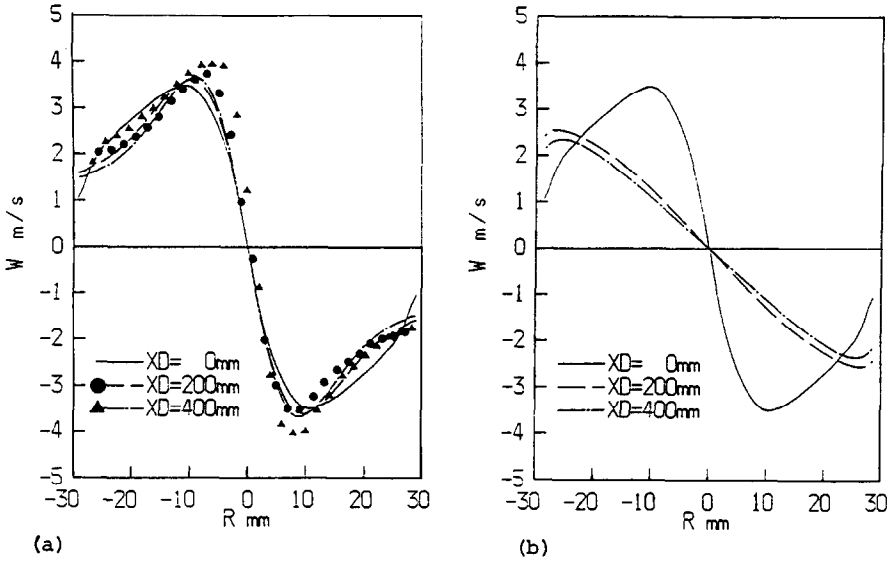

FIG. 3. Comparison of experimental and calculated tangential velocity profile. Plots, Yamada's experimental results [14]. Lines, predictions: (a) stress/flux equation model; (b) k–ε two equation model.

($i = 1, 2, \ldots$) denote the terms in equation (13), which are shown beside Fig. 4, respectively.

In the region where the tangential component W shows a solid-body rotational profile, the turbulent transport of the tangential momentum in the radial direction, $\rho\overline{vw}$, becomes nearly zero in the present calculation. Therefore, the solid-body rotational profile tends to be retained in the downstream region.

In the region where the tangential velocity W shows a free vortex profile, the production terms $P_{\overline{vw},1}$ ($= -\overline{v^2}\partial W/\partial r$) and $P_{\overline{vw},2}$ ($= \overline{w^2}\partial W/\partial r$) take positive values, which have the effect of transporting the tangential momentum toward the pipe wall. The redistribution term $R_{\overline{vw},7}$ ($= -\gamma k(\partial W/\partial r - W/r)$) has a similar effect to $P_{\overline{vw},1}$ and $P_{\overline{vw},2}$. $R_{\overline{vw},2}$ ($= \alpha\overline{v^2}\partial W/\partial r$) and $R_{\overline{vw},3}$ ($-\alpha\overline{w^2}W/r$) take negative values, which never overcome the values of $P_{\overline{vw},1}$ and $P_{\overline{vw},2}$, respectively. On the other hand, $C_{\overline{vw}}$ ($= -(\overline{v^2} - \overline{w^2})W/r$), in

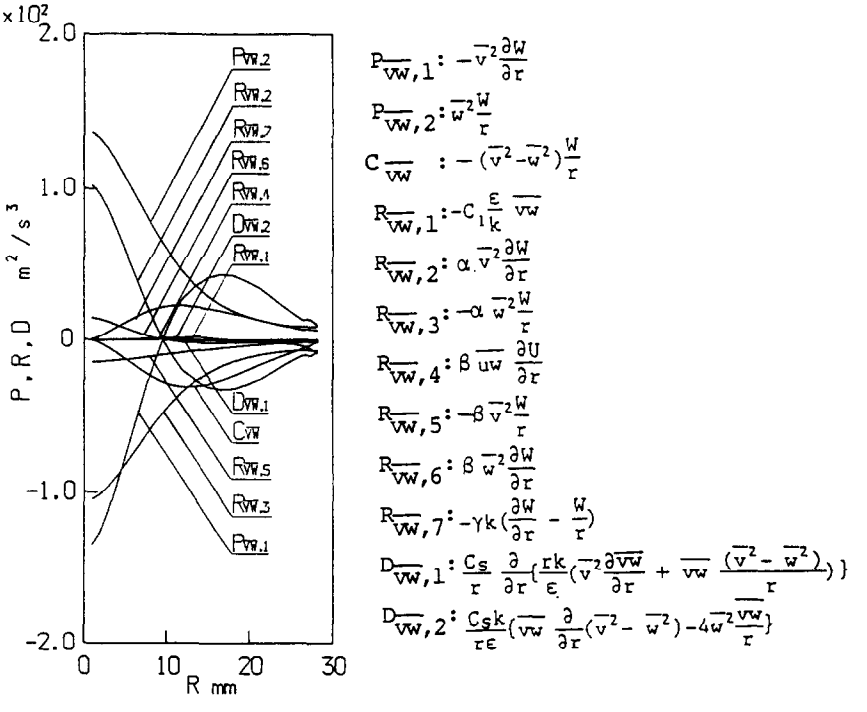

FIG. 4. Calculated radial profile of the magnitude of the terms in the transport equation of $\overline{vw}$.

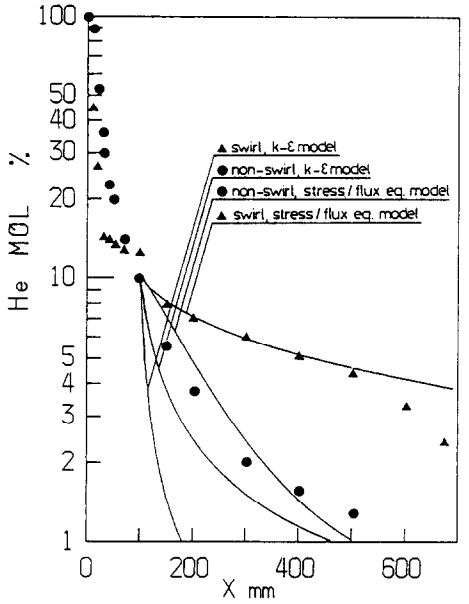

FIG. 5. Comparison of experimental and calculated concentration of He along the central axis. Plots, experimental results of ref. [13]. Lines, predictions.

the convection terms, takes a negative value, which has the effect of transporting the tangential momentum toward the central axis. Other terms in the transport equation $\overline{vw}$ are smaller than these terms. The free vortex profile retained downstream is considered to be caused by the negative term $-(\overline{v^2}-\overline{w^2})W/r$, including the anisotropy between $\overline{v^2}$ and $\overline{w^2}$.

In Fig. 5, the experimental and calculated concentrations of He along the central axis are compared. Plotted points in Fig. 5 are the experimental values of ref. [13]. The lines in Fig. 5 are the predicted ones employing the stress/flux equation model and the k–ε two equation model. X denotes the distance from the nozzle tip. The calculation starts from $X = 100$ mm ($XD = 0$). As for the non-swirling flow, the calculation employing both the k–ε turbulence model and the stress/flux equation model can predict the experimental concentration of He. As for the swirling flow, however, the experimental results show the retardation of turbulent mixing as compared with the case of the non-swirling flow. The calculation employing the stress/flux equation model predicts the concentration profile and the retardation phenomena fairly well, whereas the calculation employing the k–ε model fails to predict the phenomena. In Fig. 6 the calculated radial profiles of the concentrations of He employing the stress/flux equation model (Fig. 6(a)) and the k–ε model (Fig. 6(b)) for the swirling flow are compared with the experiments [14], respectively. The calculated profiles of He concentration using the k–ε model are flattened more rapidly as compared with the experimental values, whereas the calculations employing the stress/flux equation model predict the experimental ones fairly well. The calculation employing the stress/flux equation model estimates the turbulent transport of He in the radial direction $\rho\overline{vm}$ less than that of the k–ε model. In order to investigate the cause of the retardation of the turbulent mixing due to the swirl, the radial profile of the magnitude of the terms in the transport equation of $\overline{vm}$, equation (16), at the cross section of $XD = 200$ mm are indicated in Fig. 7. The marks in the figure $P_{\overline{vm},i}$, $R_{\overline{vm},i}$, $C_{\overline{vm},i}$ and $D_{\overline{vm},i}$ ($i = 1, 2, \ldots$) indicate the terms of equation (16), which are shown beside Fig. 7, respectively.

$P_{\overline{vm},i}$ are the production terms. $P_{\overline{vm},1}$ ($= -\overline{v^2}\partial M/\partial r$) is concerned with the radial gradient of the time-mean concentration of He and contributes significantly to the production of $\overline{vm}$. $P_{\overline{vm},1}$ has an effect on the concentration of He to diffuse in the radial direction. Particularly, in the case with the swirl, $P_{\overline{vm},2}$ ($= \overline{wm}W/r$) becomes a negative production term, which reduces the magnitude of $\overline{vm}$ and has an effect to retard the turbulent transport of He. $R_{\overline{vm},3}$ ($= -C_{2c}\overline{wm}W/r$) has an effect to produce $\overline{vm}$. But the coefficient C_{2c} takes the value 0.33 and so it never

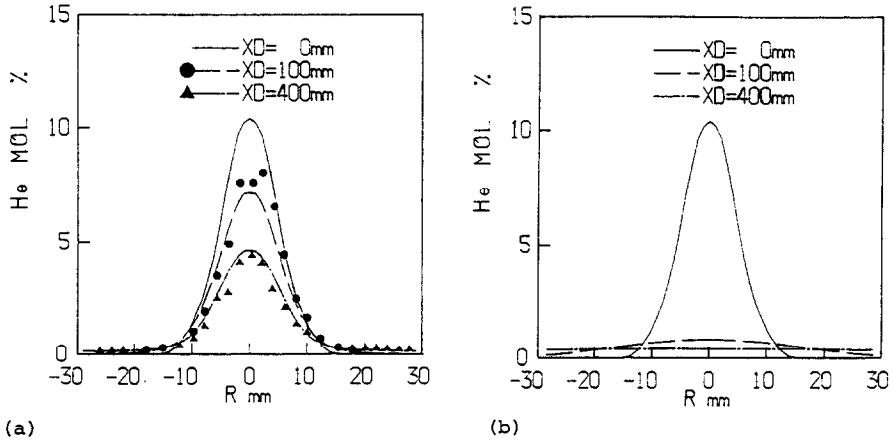

FIG. 6. Comparison of experimental and calculated radial profile of concentration of He. Plots, Yamada's experimental results [14]. Lines, predictions: (a) stress/flux equation model; (b) k–ε two equation model.

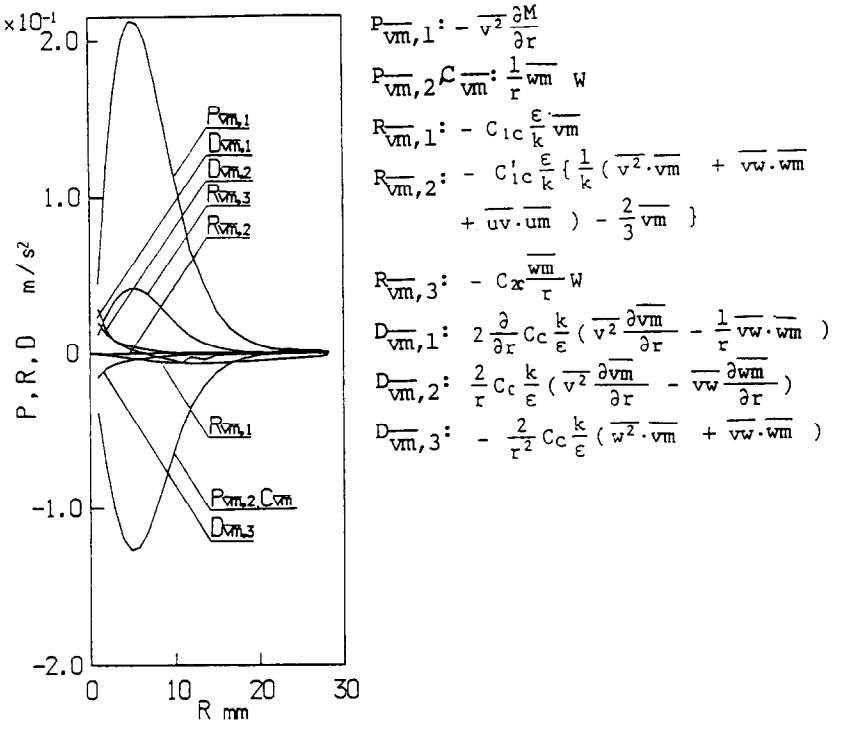

FIG. 7. Calculated radial profile of the magnitude of the terms in the transport equation of $\overline{vm}$.

overcomes the effect of $P_{\overline{vm},2}$ to suppress $\overline{vm}$. Other terms in the transport equations of $\overline{vm}$ are smaller than these terms. Hence, the negative production term $P_{\overline{vm},2}$ ($= \overline{wm}W/r$) in the stress/flux equation model predicts the retardation of the turbulent mixing due to the swirl. The same term $C_{\overline{vm}}$ ($= \overline{wm}W/r$) is contained in the convection terms.

4. SUMMARY

Computations on the turbulent swirling flow and mixing in a stationary pipe were conducted to investigate the applicability of the turbulence models and to study the causes of the swirling flow characteristics and of the retardation of mixing due to the swirl. Two kinds of turbulence models, the stress/flux equation model and the k–ε turbulence model, were applied and the computations were compared with the experiments. The results obtained in this study are as follows.

(1) The calculation employing the stress/flux equation model can predict the experimental turbulent swirling flow characteristics such that the axial velocity profile retains profiles depressed near the central axis in the downstream region and the tangential velocity profile becomes the solid-body rotational profile near the central axis and the free vortex profile at the outer region. The calculation employing the k–ε two equation model fails to predict these characteristics. The success of the prediction employing the stress/flux equation model comes from the effects of the terms $\overline{uw}W/r$ and $-(\overline{v^2}-\overline{w^2})W/r$ in the transport equations of $\overline{uv}$ and $\overline{vw}$, respectively.

(2) The stress/flux equation model can predict the phenomena of the retardation of mixing due to the swirl as compared with the non-swirling flow, whereas the k–ε two equation model fails to predict it. The negative production term $\overline{wm}W/r$ in the transport equation of $\overline{vm}$ plays important roles on the suppression of the turbulent mass transport in the radial direction.

REFERENCES

1. J. Cannon and W. Kays, Heat transfer to a fluid flowing inside a pipe rotating about its longitudinal axis, *J. Heat Transfer* **91,** 135–139 (1969).
2. K. Kikuyama, M. Murakami, K. Nishibori and K. Maeda, Flow in a rotating pipe (a calculation of flow in the saturated region), *Bull. Japan Soc. Mech. Engng* **26,** 506–513 (1983).
3. S. Hirai, T. Takagi and M. Matsumoto, Prediction of the laminarization phenomena in turbulent swirling flows, *Trans. Japan Soc. Mech. Engng* **52,** 1608–1616 (1986).
4. S. Hirai and T. Takagi, Predictions of heat transfer deterioration in turbulent swirling pipe flow, *Proc. 2nd ASME/JSME Thermal Engng Joint Conf.*, Vol. 5, pp. 181–187 (1987).
5. S. Hirai, T. Takagi, K. Tanaka and T. Higashiya, Turbulent heat transfer to the flow in a concentric annulus with a rotating inner cylinder, 8th Int. Heat Transfer Conf., Vol. 3, pp. 895–900 (1986).
6. B. E. Launder, C. H. Priddin and B. I. Sharma, The calculation of turbulent boundary layers of spinning and curved surfaces, *J. Fluids Engng* **99,** 231–239 (1977).
7. M. A. Leschziner and W. Rodi, Computation of strongly

swirling axisymmetric free jets, *AIAA J.* **22,** 1742–1747 (1984).
8. B. E. Launder and A. Morse, Numerical prediction of axisymmetric free shear flows with a second-order Reynolds stress turbulence closure. In *Turbulent Shear Flow* (Edited by F. Durst), Vol. 1, pp. 279–294. Springer, Berlin (1979).
9. M. M. Gibson and B. A. Younis, Calculation of swirling jets with a Reynolds stress closure, *Physics Fluids* **29,** 38–48 (1986).
10. G. J. Sturgess and S. A. Syed, Calculation of confined swirling flows, Paper AIAA 85-0060 (1985).
11. T. Kobayashi and M. Yoda, Modified k–ε model for turbulent swirling flow in a straight pipe, *JSME Int. J.* **30,** 66–71 (1987).
12. T. Takagi, T. Okamoto, M. Taji and Y. Nakasuji, Retardation of mixing and counter-gradient diffusion in a swirling flame, 20th Symp. (Int.) on Combustion, pp. 251–258 (1984).
13. T. Takagi, T. Okamoto and M. Yamada, Phenomena of the retardation of mixing and combustion in swirling flows, *Proc. ASME/JSME Thermal Engng Joint Conf.*, Vol. 4, pp. 131–136 (1983).
14. M. Yamada, The study of mixing and combustion in swirling flows, Master's Thesis, Osaka University (1982).
15. W. P. Jones and B. E. Launder, The calculation of low Reynolds number phenomena with a two-equation model of turbulence, *Int. J. Heat Mass Transfer* **16,** 1119–1130 (1973).
16. B. E. Launder, G. J. Reece and W. Rodi, Progress in the development of a Reynolds-stress turbulence closure, *J. Fluid Mech.* **68,** 537–566 (1975).
17. B. E. Launder, *Turbulence* (Edited by P. Bradshaw), pp. 232–289. Springer, Berlin (1976).
18. B. E. Launder and D. B. Spalding, *Mathematical Models of Turbulence*, pp. 90–110. Academic Press, New York (1972).
19. T. Takagi and S. Koto, Computation and its comparison with experiments of time-mean and fluctuating properties in round jets with and without flame, *Proc. 3rd Symp. Turbulent Shear Flows*, pp. 3.21–3.26 (1981).
20. B. J. Daly and F. H. Harlow, Transport equations in turbulence, *Physics Fluids* **13,** 2634–2649 (1970).
21. K. Hanjalic and B. E. Launder, A Reynolds stress model of turbulence and its application to thin shear flows, *J. Fluid Mech.* **52,** 609–638 (1972).
22. A. Morse, Axisymmetric free shear flows with and without swirl, Ph.D. Thesis, University of London, pp. 122–209 (1980).
23. H. Shlichting, *Boundary Layer Theory*, 4th Edn, pp. 553–558. McGraw-Hill, New York (1968).
24. S. V. Patanker and D. B. Spalding, *Heat and Mass Transfer in Boundary Layers*, pp. 28–46. Intertext Book (1970).

PREDICTION NUMERIQUE DES CARACTERISTIQUES D'ECOULEMENT ET DU RETARDEMENT DU MELANGE DANS UN ECOULEMENT TURBULENT TOURBILLONNAIRE

Résumé—Des prédictions numériques sont comparées avec les expériences, sur un écoulement turbulent tourbillonnaire et sur le mélange dans un tuyau fixe. Deux sortes de modeles de turbulence, le modèle k–ε à deux équations et le modèle à équation contrainte/flux, sont employés dans ces calculs. Les profils de vitesses axiale et tangentielle et les caractéristiques du retardement du mélange en présence du swirl peuvent être prédits par le modèle contrainte/flux, tandis que le modèle k–ε ne le peut pas. Des interprétations de ce phénomène sont présentées, spécialement sur le retardement du transfert turbulent de la quantité de mouvement et des espèces (He) dû au swirl.

NUMERISCHE BERECHNUNG DER STRÖMUNG UND DER BEHINDERUNG DER MISCHUNG IN EINER TURBULENTEN WIRBELSTRÖMUNG

Zusammenfassung—Numerische und experimentelle Ergebnisse für eine turbulente Wirbelströmung und deren Mischungsvorgänge in einem Rohr werden verglichen. Zwei unterschiedliche Turbulenz-Modelle werden in den vorliegenden Berechnungen untersucht. Bei der Bestimmung der axialen und radialen Geschwindigkeitsprofile und der Behinderung der Mischung in Gegenwart von Wirbeln ergeben sich bei der Anwendung des k–ε-Zwei-Gleichungsmodells Fehler. Interpretationen der Phänomene, insbesondere der Behinderung des turbulenten Impuls- und Stofftransports infolge der Wirbel, werden vorgestellt.

ЧИСЛЕННЫЙ РАСЧЕТ ХАРАКТЕРИСТИК ТЕЧЕНИЯ И ЗАМЕДЛЕНИЯ СМЕШЕНИЯ В ТУРБУЛЕНТНОМ ЗАКРУЧЕННОМ ПОТОКЕ

Аннотация—Проведено сравнение численных расчетов с экспериментальными данными по турбулентному закрученному потоку и смешению в неподвижной трубе. При расчетах использовались два вида моделей турбулентности: двухпараметрическая модель k–ε и модель для напряжений Рейнольдса. Показано, что профили осевой и тангенциальной скорости и характеристики замедления смешения при наличии закрутки можно рассчитать только с помощью второй модели. Дано подробное объяснение наблюдаемых явлений, в особенности замедления турбулентного переноса количества движения и вещества, вызванного закруткой.